Highly Efficient Electron Transfer in a Carbon Dot - Polyoxometalate Nanohybrid

Antonino Madonia,[†] Mercè Martin-Sabi,[†] Alice Sciortino,[‡] Simonpietro Agnello,[‡,¶] Marco Cannas,[‡] Souad Ammar,[†] Fabrizio Messina,[*,‡,¶] and Delphine Schaming[*,†]

†*Université de Paris, ITODYS, CNRS, UMR 7086, 15 rue J-A de Baïf, 75013 Paris, France*

‡*DiFC, Università degli Studi di Palermo, via Archirafi 36, 96100 Palermo, Italy*

¶*CHAB – ATeN Center, Università degli Studi di Palermo, Viale delle Scienze, Edificio 18, 90128 Palermo, Italy.*

E-mail: fabrizio.messina@unipa.it; delphine.schaming@u-paris.fr

Abstract

Using solar radiation to fuel catalytic processes is often regarded as the solution to our energy needs. However, developing effective photocatalysts active under visible light has proven to be difficult, often due to toxicity, instability, and high cost of suitable catalysts. We engineered a novel photoactive nanomaterial obtained by the spontaneous electrostatic coupling of carbon nanodots with $[P_2W_{18}O_{62}]^{6-}$, a molecular catalyst belonging to the class of polyoxometalates. While the former are used as photosensitizers, the latter was chosen for its ability to catalyze reductive reactions such as dye decomposition and water-splitting. We find the electron transfer within the nanohybrid to be so efficient that a charge-separated state is formed within 120 femtoseconds from photon absorption. These results are a cornerstone towards the engineering of a new class of nano-devices, non-toxic, low-cost, and able to carry out solar-driven catalytic processes.

Graphical TOC Entry

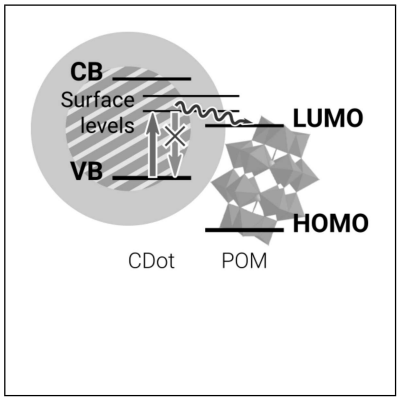

Keywords

Polyoxometalates, Carbon Dots, Electron Transfer, Ultrafast Spectroscopy

Due to the problems associated to the use of fossil fuels, the interest in light-driven physicochemical processes continues to grow. Because of the ready availability of solar radiation, many efforts have been focused on developing means to harvest and convert this energy.[1] Photocatalytic processes have attracted a particular attention, due to their potential huge impact in renewable energy and environment protection.[2] However, developing stable and non-toxic nano-photocatalysts active under visible light still remains a challenge.

While several metal nano-oxides (such as TiO_2, WO_3 and ZnO) have already been used for these purposes, the last decade has seen a growing interest towards polyoxometalates (POMs), a family of nano-scaled metal oxide polyanionic clusters based on highly oxidized metals.[3] POMs are very promising in the domain of photocatalysis because of their ability to reversibly accept a large number of electrons from a donor[4–7] and have shown remarkable catalytic properties[8,9] for water-splitting[10,11] and pollutant degradation.[12] Moreover, the physical and chemical characteristics of POMs can be easily tuned by adjusting their chemical composition and structure.[3,13] Unfortunately, POMs suffer from light absorption limitations as they are only excited in the UV range.

In order to overcome this issue a common strategy consists in using visible-active photosensitizers acting as electron relays. Organic dyes, metal complexes, quantum dots and metal nanoparticles have already been coupled to POMs to extend their absorption range to the visible.[9,14–22] Nevertheless, all these sensitizers suffer from either bad stability during light irradiation[23] or high toxicity.[24–26] Therefore, the challenge is finding photosensitizers which are photostable, non-toxic and contain no expensive or rare elements.

Carbon dots (CDs), a new family of optically active nano-sized carbon materials discovered few years ago,[27] may offer a viable solution. CDs are small ($< 10\,\text{nm}$) and highly surface-functionalized nanoparticles, displaying very bright fluorescence and intense absorption bands often covering most of the visible spectrum.[28–32] These simple to synthesize[27,28,33–36] nanoparticles are found to be non-toxic both in vitro and in vivo,[34,37,38] are composed by light elements only (C, N, O, H), and are very stable under prolonged visible

illumination. Moreover, CDs can be easily coupled to other species thanks to the organic functional groups present on their surface[33,39,40] and display a strong tendency to donate electrons to interacting species via an ultrafast photo-induced electron transfer (ET), as recently demonstrated.[41] Therefore, one may argue CDs to be the ideal candidate to serve as POMs photosensitizer.

In this work we explore these ideas and propose to use CDs as sensitizers for POMs. By a careful choice of the CDs design and synthetic route we achieve their spontaneous coupling to POMs, aiming to produce efficient nanohybrid photocatalysts. This pairing is achieved in mildly acidic aqueous solution, driven by electrostatic interactions. The POM-CDs hybrids were thoroughly investigated via steady-state, nanosecond and femtosecond time-resolved optical spectroscopy. Thereby, we demonstrate an extremely efficient electron transfer from CDs to POMs, occurring within 120 femtoseconds from photo-excitation, a very promising result for a whole range of photocatalytic applications.

The metal oxide cluster we decided to use towards the development of POM-CDs hybrid systems is the well known[42] Dawson-structured $[P_2W_{18}O_{62}]^{6-}$, obtained via an already reported synthetic procedure[43] and characterized by ^{31}P NMR (Figure S2). This POM was chosen for its capability to accept a high number of electrons and because it is an archetype for the whole family of polyoxometalates.

CDs were synthesized in an autoclave by a bottom-up approach[44] (detailed in the SI) which yields cyan-fluorescent CDs. These nanoparticles display a graphitic core structure, as confirmed by the D and G bands found in the Raman spectrum[44] (G to D intensity ratio of 1.2, Figure 1A). As observed via AFM (Figure 1B), they display an approximately spherical shape with an average height of 3.7 nm and a standard deviation of 2.0 nm. The surface, studied by FTIR spectroscopy, is rich in organic moieties most of which are amines (Figure 1C and Table S1). In solution, the vast majority of CDs reported in the literature display a negative surface charge[45] that would hinder their coupling to POM anions, because of electrostatic repulsion. In contrast, a key feature of the CDs produced here is the possibility

of varying their surface charge depending on pH, thanks to the organic groups present on the outer shell. Indeed, according to zeta (ζ) potential measurements shown in Figure 1D, the CDs surface is positively charged at pH < 4 (CDs^+), due to the protonation of the surface amino groups. In these conditions, CDs should be able to couple to polyanionic POMs thanks to their opposite charges.

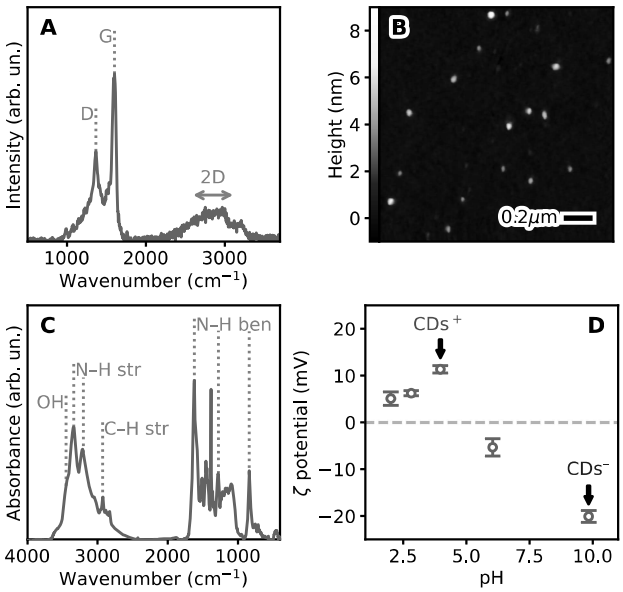

Figure 1: CDs structural characterization. A) Raman spectrum of CDs obtained at $\lambda_{exc} = 325\,\text{nm}$; graphitic carbon characteristic bands are indicated; B) AFM topography of CDs reveals approximately spherical particles of 3.7 nm average height ($\sigma = 2.0\,\text{nm}$); C) the FTIR spectrum of CDs allows the identification of their amine-coated surface; stretching and bending vibration peaks are indicated as *str* and *ben*. D) The measured ζ potential of a CDs solution as a function of pH shows that the surface charge of the nanoparticles can be controlled.

The optical properties of CDs are summarized in Figure 2. The study has been conducted on both negative (CDs^-, pH=10) and positive (CDs^+, pH=4) particles. A strong absorption, ideal for harvesting solar light, is observed at the blue end of the visible spectrum for CDs^-, while reaching up to 500 nm for CDs^+. Under excitation at 400 nm, their fluorescence (Figure 2A) peaks at 480 and 460 nm with emission quantum yields (QY) estimated to be 36% and 11% for CDs^- and CDs^+ respectively. Time resolved emission spectroscopy (Figure 2B) allows to measure lifetimes τ equal to $5.7 \pm 0.2\,\text{ns}$ (CDs^-) and $5.3 \pm 0.2\,\text{ns}$ (CDs^+).

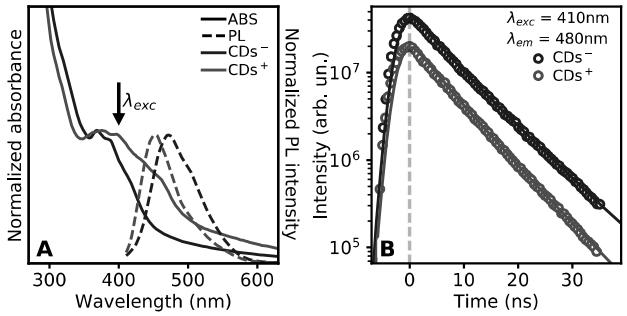

Figure 2: CDs optical characterization. A) Normalized steady state UV-visible absorption spectra (full line) and fluorescence spectra ($\lambda_{exc} = 400\,\text{nm}$, dashed line) of CDs^- and CDs^+; B) Emission decay traces obtained via time resolved emission spectroscopy of CDs^- and CDs^+ ($\lambda_{exc} = 410\,\text{nm}$, $\lambda_{em} = 480\,\text{nm}$).

We observe minor but relevant differences between the optical properties of the two oppositely charged CDs (Figure 2A and B), such as a change in lifetime and a shift in both absorption and emission bands. These changes indicate the key involvement of surface chemical groups in the optical transitions of these nanoparticles, considering that the charge state depends on the protonation/deprotonation of surface moieties controlled by pH. Indeed, the direct involvement of surface moieties in the photocycle of these CDs is expected to favor the electron transfer to POMs, as demonstrated hereafter.

The spontaneous formation of POM-CDs electrostatic hybrids is quickly obtained by adding POMs to a CDs solution, as revealed by fluorescence quenching (Figure 3). This effect is way more pronounced for CDs^+, with an emission intensity decrease of 75% at a concentration of POMs as small as $5.8\,\mu\text{M}$ (Figure 3A). Reversely, only a very small effect is observed when POMs are added to CDs^-. This can be interpreted as the spontaneous formation of an electrostatic pair composed by polyanionic POMs and CDs^+, wherein the CDs fluorescence is quenched by an electron transfer to POMs. AFM analysis of the sample after coupling suggests coverage of the CDs surface by a $1-2\,\text{nm}$ thick layer of POMs (Figure S10).

The fluorescence quenching observed at different $[P_2W_{18}O_{62}]^{6-}$ concentrations (Figure 3B) can be analyzed by Stern-Volmer plots,[46] as presented in Figure 3C. The quenching of CD^+

is characterized by two separate regimes, observed as different slopes in the Stern-Volmer plot at low ($< 10\,\mu M$) and high ($> 10\,\mu M$) POMs concentration. Least-squares fits (Table S2) yield quenching constants of $2.4 \times 10^6\,M^{-1}$ and $6.1 \times 10^3\,M^{-1}$ for the interaction between CDs^+ and POMs, suggesting two chemically different interaction sites available for POMs at the surface of CDs^+. Moreover, these values are much higher than the diffusion limited quenching constants ($90\,M^{-1}$, see SI and Table S3). This discrepancy confirms that the quenching is static, that is, occurring within the stable POM^--CDs^+ complexes formed by electrostatic interaction. The static coupling of these species is conclusively confirmed by time resolved fluorescence spectroscopy by observing the same emission dynamics at all $[P_2W_{18}O_{62}]^{6-}$ concentrations: as shown in Figure 3D, all decay curves are parallel to each other in a logarithmic y-scale, implying a constant lifetime. This lack of changes (further confirmed in Figure S13 and Table S4) conclusively rules out a collisional quenching, which

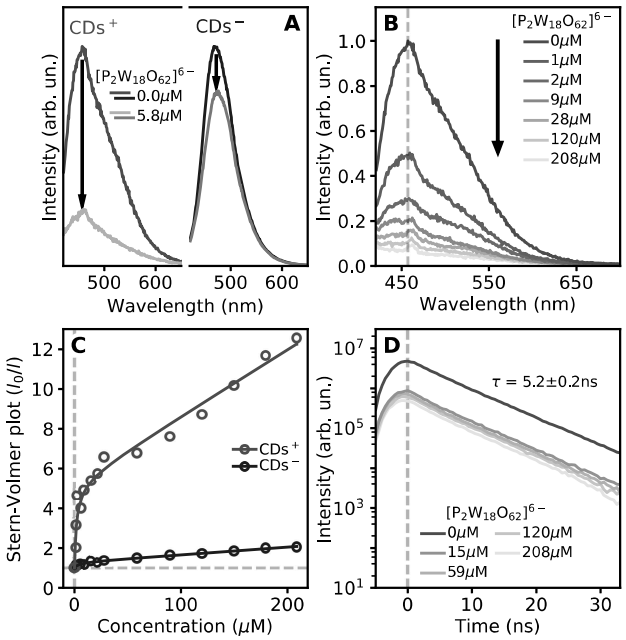

Figure 3: Quenching of CDs emission in solution by $[P_2W_{18}O_{62}]^{6-}$. A) Effect of a same quantity of POMs on the emission of CDs^+ and CDs^-; B) Emission spectra of CDs^+ after addition of POMs at different concentrations; C) Stern-Volmer plot of the CDs^+ and CDs^- emission when quenched by $[P_2W_{18}O_{62}]^{6-}$; D) Emission decay traces of CDs^+ after addition of POMs at different concentrations. The measured lifetime, equal for all traces, is reported.

would reflect in a decrease of the lifetime, and proves that the electron transfer from CD^+ to POMs is so efficient to occur on a sub-nanosecond time scale.

The fast interaction was therefore studied by femtosecond transient absorption (TA) experiments excited by 400 nm pulses of 75 fs duration. We carried out three TA experiments on CDs^+ in solution, before and after the addition of POMs at 1.25 µM (Figure 4) and 125 µM (shown in the SI) concentration. Figure 4A and 4B display the TA spectra of CDs^+ and 1.25 µM POM-CDs^+ solutions as a function of pump-probe delay where four main contributions are identified: the negative signal below 410 nm, close to the pump wavelength, is assigned to ground-state bleaching (GSB); the strong peaks at 460 nm and 590 nm are due to excited state absorption (ESA); finally, the stimulated emission (SE) signal can be recognized in the dip showing up at $\sim$ 500 nm in all spectra. This last feature resembles the steady-state fluorescence in Figure 2A although reversed in sign, which is the typical fingerprint of SE signals in TA spectra.[41]

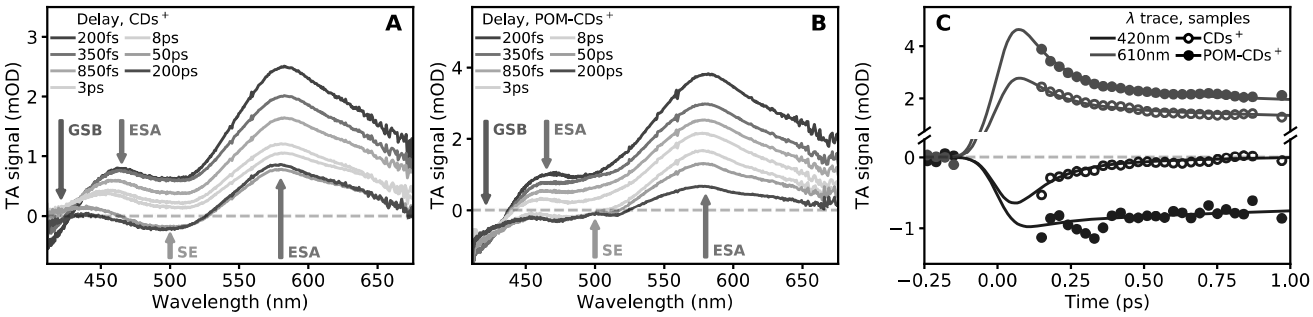

Figure 4: Ultrafast transient absorption of CDs^+ and POM-CDs^+ complexes. A) and B) TA spectra at different excitation delays of CDs^+ and POM-CDs^+ respectively; arrows indicate the GSB (in blue), SE (in green), and ESA (in red) signals. C) TA decay traces and their fits at 420 nm and 610 nm for CDs^+ and POM-CDs^+.

Some important differences appear between the two samples. At all time delays, the SE signal in CDs^+ (Figure 4A) is stronger than in POM-CDs^+ (Figure 4B). In the latter, the dip around 500 nm is barely visible at all times, as observed in Figure 4 and S15. Being SE equivalent to fluorescence, this finding provides another evidence of the quenching of CDs^+ by POMs, consistent with Figure 3. Furthermore, the SE signal in POM-CDs^+ is

already much weaker than in CDs^+ since early delays, suggesting that the ET is so efficient to happen faster than the 120 fs time resolution. This conclusion is confirmed by comparing the GSB behavior, represented by the 420 nm TA traces presented in Figure 4C. This signal severely decays within a few hundreds femtoseconds in CDs^+, likely due to a non-radiative decay back to the ground state. In POM-CDs^+, the GSB decay can now be used as an internal clock allowing us to deduce that the ET must be much faster than it. Indeed, we observe that the GSB is much longer lived in POM-CDs^+, with almost no decay occurring in the first ps (Figure 4C) and most of the signal surviving for hundreds of picoseconds (Figure S17). This difference can again be explained by a very efficient ET preventing non-radiative recombinations: in POM-CDs^+, the photoexcited CDs^+ immediately (< 120 fs) lose an electron due to ET towards POMs. Therefore, their ground-state can not be repopulated and the GSB does not decay, explaining the longer-lived signal.

Finally, we carried out a global multi-exponential fitting of the four traces in Figure 4C and found that they are described by a set of four time components identical for both samples: $\tau_1 = 120 \pm 13$ fs, $\tau_2 = 1.8 \pm 0.2$ ps, $\tau_3 = 110 \pm 30$ ps and $\tau_4 > 1$ ns. The only difference between the pump-probe dynamics of the samples thus lies in the pre-exponential fitting amplitudes (Table S5) rather than in the time scales and, as such, the traces recorded with and without POMs are related to each other by a simple linear normalization (Figure S18). The lack of any new component related to ET dynamics appearing in POM-CDs^+ conclusively confirms that the ET occurs faster than 120 fs. As shown in the SI, results obtained at the higher 125 µM POMs concentration follow the same trends, although TA data become less reliable because of sample aggregation and the consequent strong pump scattering.

Interestingly, our previous studies on the interaction between photo-excited CDs and model transition metal ions have found the ET to proceed at least one order of magnitude slower.[41] However, extremely fast ETs such as the one observed here between CDs and POMs are not uncommon in other systems[47] and indicate an extremely efficient electronic coupling within the complexes.

In conclusion, the results herein reported provide evidence of a spontaneous electrostatic coupling between POMs and CDs obtained in very mild acidic conditions. As seen via ultrafast transient absorption spectroscopy, the sub-picosecond interaction between the two species enables a highly efficient photoinduced electron transfer. This is evidenced by a characteristic lifetime found to be smaller than the 120 fs temporal resolution of the femtosecond pump-probe setup. We believe that these results are a first step towards the development of a new class of inexpensive and efficient photocatalytic carbon-based devices. Combining the highly tunable optical properties of CDs[45] with the wide range of POMs structures and catalytic capabilities could initiate the development of a new generation of hybrids useful to catalyze processes such as water-splitting, pollutant degradation, and toxic metals reduction.

Acknowledgement

This work was supported by the institutes Université de Paris, CNRS (Centre National de Recherche Scientifique), and University of Palermo. This project has received funding from the ANR (Agence Nationale de la Recherche) (project POMDOT, post-doctoral fellowship to M.M.-S.), the city of Paris, Campus France and Università Italo Francese (Program PHC Galileo), and the European Union's Horizon 2020 research and innovation programme under the Marie Skłodowska-Curie grant agreement No 665850 (PhD fellowship to A.M.).

Supporting Information Available

The following files are available free of charge.

- SI.pdf: Contains experimental details, least-square fitting parameters of nanosecond, Stern-Volmer and TA data, additional AFM, Raman, FTIR, optical absorption and fluorescence data.

References

(1) García-Martínez, J., Serrano-Torregrosa, E., Eds. *The Chemical Element: Chemistry's Contribution to Our Global Future*; Wiley-VCH: Weinheim, 2011.

(2) Dionysiou, D. D., Li Puma, G., Ye, J., Schneider, J., Bahnemann, D., Eds. *Photocatalysis: Applications*; Energy and Environment Series; The Royal Society of Chemistry: Cambridge, 2016.

(3) Ruhlmann, L., Schaming, D., Eds. *Trends in polyoxometalates research*; Chemistry research and applications; Nova Publishers: New York, 2015.

(4) Ruhlmann, L.; Nadjo, L.; Canny, J.; Contant, R.; Thouvenot, R. Di- and Tetranuclear Dawson-Derived Sandwich Complexes: Synthesis, Spectroscopic Characterization, and Electrochemical Behavior. *Eur. J. Inorg. Chem.* **2002**, *2002*, 975–986.

(5) Ruhlmann, L.; Canny, J.; Vaissermann, J.; Thouvenot, R. Mixed-metal sandwich complexes $[M(II)_2(H_2O)_2Fe(III)_2(P_2W_{15}O_{56})_2]^{14-}$ (M(II) = Co, Mn): Synthesis and stability. The molecular structure of $[M(II)_2(H_2O)_2Fe(III)_2(P_2W_{15}O_{56})_2]^{14-}$. *Dalton Trans.* **2004**, 794–800.

(6) Schaming, D.; Canny, J.; Boubekeur, K.; Thouvenot, R.; Ruhlmann, L. An Unprecedented Trinuclear Dawson Sandwich Complex with Internal Lacuna: Synthesis and ^{31}P NMR Spectroscopic Analysis of the Symmetrical $[NaNi_3(H_2O)_2(P_2W_{15}O_{56})_2]^{17-}$ and $[CoNi_3(H_2O)_2(P_2W_{15}O_{56})_2]^{16-}$ Anions. *Eur. J. Inorg. Chem.* **2009**, *2009*, 5004–5009.

(7) Ruhlmann, L.; Schaming, D.; Ahmed, I.; Courville, A.; Canny, J.; Thouvenot, R. Spectroscopic and Electrochemical Study of the Interconversion and Decomplexation of Cobalt(II) Sandwich Polyoxometalates Based on a Dawson-Type Anion. *Inorg. Chem.* **2012**, *51*, 8202–8211.

(8) Costa-Coquelard, C.; Schaming, D.; Lampre, I.; Ruhlmann, L. Photocatalytic reduction of Ag_2SO_4 by the Dawson anion $\alpha-[P_2W_{18}O_{62}]^{6-}$ and tetracobalt sandwich complexes. *Appl. Catal., B* **2008**, *84*, 835–842.

(9) Schaming, D.; Costa-Coquelard, C.; Sorgues, S.; Ruhlmann, L.; Lampre, I. Photocatalytic reduction of Ag_2SO_4 by electrostatic complexes formed by tetracationic zinc porphyrins and tetracobalt Dawson-derived sandwich polyanion. *Appl. Catal., A* **2010**, *373*, 160–167.

(10) Bernardini, G.; Wedd, A. G.; Zhao, C.; Bond, A. M. Photochemical oxidation of water and reduction of polyoxometalate anions at interfaces of water with ionic liquids or diethylether. *Proc. Natl. Acad. Sci. U. S. A.* **2012**, *109*, 11552–11557.

(11) Yamase, T.; Cao, X.; Yazaki, S. Structure of double Keggin-Ti/W-mixed polyanion $[(A-\beta-GeTi_3W_9O_{37})_2O_3]^{14-}$ and multielectron-transfer-based photocatalyic H_2-generation. *J. Mol. Catal. A: Chem.* **2007**, *262*, 119–127.

(12) Antonaraki, S.; Triantis, T.; Papaconstantinou, E.; Hiskia, A. Photocatalytic degradation of lindane by polyoxometalates: Intermediates and mechanistic aspects. *Catal. Today* **2010**, *151*, 119–124.

(13) Martin-Sabi, M.; Soriano-López, J.; Winter, R. S.; Chen, J.-J.; Vilà-Nadal, L.; Long, D.-L.; Galán-Mascarós, J. R.; Cronin, L. Redox tuning the Weakley-type polyoxometalate archetype for the oxygen evolution reaction. *Nat. Catal.* **2018**, *1*, 208–213.

(14) Schaming, D.; Allain, C.; Farha, R.; Goldmann, M.; Lobstein, S.; Giraudeau, A.; Hasenknopf, B.; Ruhlmann, L. Synthesis and Photocatalytic Properties of Mixed Polyoxometalate-Porphyrin Copolymers Obtained from Anderson-Type Polyoxomolybdates. *Langmuir* **2010**, *26*, 5101–5109.

(15) Schaming, D.; Costa-Coquelard, C.; Lampre, I.; Sorgues, S.; Erard, M.; Liu, X.; Liu, J.; Sun, L.; Canny, J.; Thouvenot, R. et al. Formation of a new hybrid complex via coor-

dination interaction between 5,10,15-tritolyl-20-(4- and 3-pyridyl)porphyrin or 5,10,15-triphenyl-20-(4-pyridyl)porphyrin and the $\alpha-[MSiW_{11}O_{39}]^{6-}$ Keggin-type polyoxometalate (M=Co^{2+} and Ni^{2+}). *Inorg. Chim. Acta* **2010**, *363*, 2185–2192.

(16) Schaming, D.; Farha, R.; Xu, H.; Goldmann, M.; Ruhlmann, L. Formation and Photocatalytic Properties of Nanocomposite Films Containing Both Tetracobalt Dawson-Derived Sandwich Polyanions and Tetracationic Porphyrins. *Langmuir* **2011**, *27*, 132–143.

(17) Car, P.-E.; Guttentag, M.; Baldridge, K. K.; Alberto, R.; Patzke, G. R. Synthesis and characterization of open and sandwich-type polyoxometalates reveals visible-light-driven water oxidation via POM-photosensitizer complexes. *Green Chem.* **2012**, *14*, 1680–1688.

(18) Allain, C.; Schaming, D.; Karakostas, N.; Erard, M.; Gisselbrecht, J.-P.; Sorgues, S.; Lampre, I.; Ruhlmann, L.; Hasenknopf, B. Synthesis, electrochemical and photophysical properties of covalently linked porphyrin–polyoxometalates. *Dalton Trans.* **2013**, *42*, 2745–2754.

(19) Walsh, J. J.; Bond, A. M.; Forster, R. J.; Keyes, T. E. Hybrid polyoxometalate materials for photo(electro-) chemical applications. *Coord. Chem. Rev.* **2016**, *306*, 217–234.

(20) Schönweiz, S.; Rommel, S. A.; Kübel, J.; Micheel, M.; Dietzek, B.; Rau, S.; Streb, C. Covalent Photosensitizer-Polyoxometalate-Catalyst Dyads for Visible-Light-Driven Hydrogen Evolution. *Chem. Eur. J.* **2016**, *22*, 12002–12005.

(21) Black, F. A.; Jacquart, A.; Toupalas, G.; Alves, S.; Proust, A.; Clark, I. P.; Gibson, E. A.; Izzet, G. Rapid photoinduced charge injection into covalent polyoxometalate–bodipy conjugates. *Chem. Sci.* **2018**, *9*, 5578–5584.

(22) Soriano-López, J.; Song, F.; Patzke, G. R.; Galan-Mascaros, J. R. Photoinduced Oxygen

Evolution Catalysis Promoted by Polyoxometalate Salts of Cationic Photosensitizers. *Front. Chem.* **2018**, *6*, 302.

(23) Meissner, D.; Memming, R.; Kastening, B. Photoelectrochemistry of cadmium sulfide. 1. Reanalysis of photocorrosion and flat-band potential. *J. Phys. Chem.* **1988**, *92*, 3476–3483.

(24) Michalet, X. Quantum Dots for Live Cells, in Vivo Imaging, and Diagnostics. *Science* **2005**, *307*, 538–544.

(25) Derfus, A. M.; Chan, W. C. W.; Bhatia, S. N. Probing the Cytotoxicity of Semiconductor Quantum Dots. *Nano Lett.* **2004**, *4*, 11–18.

(26) Kirchner, C.; Liedl, T.; Kudera, S.; Pellegrino, T.; Muñoz Javier, A.; Gaub, H. E.; Stölzle, S.; Fertig, N.; Parak, W. J. Cytotoxicity of Colloidal CdSe and CdSe/ZnS Nanoparticles. *Nano Lett.* **2005**, *5*, 331–338.

(27) Sun, Y.-P.; Zhou, B.; Lin, Y.; Wang, W.; Fernando, K. A. S.; Pathak, P.; Meziani, M. J.; Harruff, B. A.; Wang, X.; Wang, H. et al. Quantum-Sized Carbon Dots for Bright and Colorful Photoluminescence. *J. Am. Chem. Soc.* **2006**, *128*, 7756–7757.

(28) Zhu, H.; Wang, X.; Li, Y.; Wang, Z.; Yang, F.; Yang, X. Microwave synthesis of fluorescent carbon nanoparticles with electrochemiluminescence properties. *Chem. Comm.* **2009**, 5118–5120.

(29) Ma, Z.; Ming, H.; Huang, H.; Liu, Y.; Kang, Z. One-step ultrasonic synthesis of fluorescent N-doped carbon dots from glucose and their visible-light sensitive photocatalytic ability. *New J. Chem.* **2012**, *36*, 861–864.

(30) Sciortino, A.; Marino, E.; Dam, B. v.; Schall, P.; Cannas, M.; Messina, F. Solvatochromism Unravels the Emission Mechanism of Carbon Nanodots. *J. Phys. Chem. Lett.* **2016**, *7*, 3419–3423.

(31) Messina, F.; Sciortino, L.; Popescu, R.; Venezia, A. M.; Sciortino, A.; Buscarino, G.; Agnello, S.; Schneider, R.; Gerthsen, D.; Cannas, M. et al. Fluorescent nitrogen-rich carbon nanodots with an unexpected $\beta-C_3N_4$ nanocrystalline structure. *J. Mater. Chem. C* **2016**, *4*, 2598–2605.

(32) Sciortino, A.; Mauro, N.; Buscarino, G.; Sciortino, L.; Popescu, R.; Schneider, R.; Giammona, G.; Gerthsen, D.; Cannas, M.; Messina, F. $\beta-C_3N_4$ Nanocrystals: Carbon Dots with Extraordinary Morphological, Structural, and Optical Homogeneity. *Chem. Mater.* **2018**, *30*, 1695–1700.

(33) Li, H.; He, X.; Kang, Z.; Huang, H.; Liu, Y.; Liu, J.; Lian, S.; Tsang, C.; Yang, X.; Lee, S.-T. Water-Soluble Fluorescent Carbon Quantum Dots and Photocatalyst Design. *Angew. Chem., Int. Ed.* **2010**, *49*, 4430–4434.

(34) Qu, S.; Wang, X.; Lu, Q.; Liu, X.; Wang, L. A Biocompatible Fluorescent Ink Based on Water-Soluble Luminescent Carbon Nanodots. *Angew. Chem., Int. Ed.* **2012**, *51*, 12215–12218.

(35) Liu, H.; Ye, T.; Mao, C. Fluorescent Carbon Nanoparticles Derived from Candle Soot. *Angew. Chem., Int. Ed.* **2007**, *46*, 6473–6475.

(36) Liu, R.; Wu, D.; Liu, S.; Koynov, K.; Knoll, W.; Li, Q. An Aqueous Route to Multicolor Photoluminescent Carbon Dots Using Silica Spheres as Carriers. *Angew. Chem., Int. Ed.* **2009**, *48*, 4598–4601.

(37) Yang, S.-T.; Cao, L.; Luo, P. G.; Lu, F.; Wang, X.; Wang, H.; Meziani, M. J.; Liu, Y.; Qi, G.; Sun, Y.-P. Carbon Dots for Optical Imaging in Vivo. *J. Am. Chem. Soc.* **2009**, *131*, 11308–11309.

(38) Hsu, P.-C.; Chen, P.-C.; Ou, C.-M.; Chang, H.-Y.; Chang, H.-T. Extremely high inhibition activity of photoluminescent carbon nanodots toward cancer cells. *J. Mater. Chem. B* **2013**, *1*, 1774–1781.

(39) Sun, M.; Ma, X.; Chen, X.; Sun, Y.; Cui, X.; Lin, Y. A nanocomposite of carbon quantum dots and TiO_2 nanotube arrays: enhancing photoelectrochemical and photocatalytic properties. *RSC Adv.* **2014**, *4*, 1120–1127.

(40) Suzuki, K.; Malfatti, L.; Takahashi, M.; Carboni, D.; Messina, F.; Tokudome, Y.; Takemoto, M.; Innocenzi, P. Design of Carbon Dots Photoluminescence through Organo-Functional Silane Grafting for Solid-State Emitting Devices. *Sci. Rep.* **2017**, *7*, 5469.

(41) Sciortino, A.; Madonia, A.; Gazzetto, M.; Sciortino, L.; Rohwer, E. J.; Feurer, T.; Gelardi, F. M.; Cannas, M.; Cannizzo, A.; Messina, F. The interaction of photoexcited carbon nanodots with metal ions disclosed down to the femtosecond scale. *Nanoscale* **2017**, *9*, 11902–11911.

(42) Briand, L. E.; Baronetti, G. T.; Thomas, H. J. The State of the Art on Wells-Dawson Heteropoly-Compounds. A Review of Their Properties and Applications. *Appl. Catal., A* **2003**, *256*, 37–50.

(43) Mbomekalle, I.-M.; Lu, Y. W.; Keita, B.; Nadjo, L. Simple, high yield and reagent-saving synthesis of pure $\alpha-K_6P_2W_{18}O_{62}\cdot 14\,H_2O$. *Inorg. Chem. Commun.* **2004**, *7*, 86–90.

(44) Wang, L.; Wang, Y.; Xu, T.; Liao, H.; Yao, C.; Liu, Y.; Li, Z.; Chen, Z.; Pan, D.; Sun, L. et al. Gram-scale synthesis of single-crystalline graphene quantum dots with superior optical properties. *Nat. Commun.* **2014**, *5*, 5357–5365.

(45) Sciortino, A.; Cannizzo, A.; Messina, F. Carbon Nanodots: A Review—From the Current Understanding of the Fundamental Photophysics to the Full Control of the Optical Response. *C* **2018**, *4*, 67.

(46) Lakowicz, J. R. *Principles of Fluorescence Spectroscopy*; Springer: New York, 2006.

(47) Wörner, H. J.; Arrell, C. A.; Banerji, N.; Cannizzo, A.; Chergui, M.; Das, A. K.; Hamm, P.; Keller, U.; Kraus, P. M.; Liberatore, E. et al. Charge migration and charge transfer in molecular systems. *Struct. Dyn.* **2017**, *4*, 061508.